PhD THESIS PROPOSAL
July 2010

MICROSTRUCTURAL CHARACTERIZATION & VISCOELASTIC PROPERTIES OF AlZnMgCu ALLOYS FOR AEROSPACE APPLICATIONS

Jose I. Rojas

PhD Advisor:
Daniel Crespo Artiaga

Doctorat en Ciència i Tecnologia Aeroespacial (DoCTA)
Universitat Politècnica de Catalunya (UPC)
Escola Politècnica Superior de Castelldefels (EPSC)
Grup de Caracterització de Materials (GCM)
Centre de Recerca de l'Aeronàutica i de l'Espai (CRAE)

CONTENTS

PhD PROPOSAL INFORMATION

PhD CANDIDATE INFORMATION

Name	José I. Rojas Gregorio
Degree	Aeronautical Engineer (ETSIA - UPM[1]) Advanced Studies Diploma (DEA[2])
Address	Escola Politècnica Superior de Castelldefels (EPSC) PMT Building C3 – Office 120 Esteve Terradas, 7 08860 - Castelldefels - Barcelona
Phone	+34 93 413 4130
Email	josep.ignasi.rojas@fa.upc.edu

PhD ADVISOR INFORMATION

Name	Daniel Crespo Artiaga
Address	Escola Politècnica Superior de Castelldefels (EPSC) PMT Building C3 – Office 112 Esteve Terradas, 7 08860 - Castelldefels - Barcelona
Phone	+34 93 413 4141
Email	daniel.crespo@upc.edu

PhD THESIS PROVISIONAL TITLE

MICROSTRUCTURAL CHARACTERIZATION & VISCOELASTIC PROPERTIES OF AlZnMgCu ALLOYS FOR AEROSPACE APPLICATIONS

[1] Escuela Técnica Superior de Ingenieros Aeronáuticos – Universidad Politécnica de Madrid.
[2] Diploma d'Estudis Avançats, DoCTA, UPC.

1 INTRODUCTION

Being aeronautics and astronautics a wide and multidisciplinary field of knowledge, materials science and technology have historically played a role of significant relevance, to such an extent that, in many cases, both have evolved together. Examples can be found everywhere: the rise of aluminium alloys and the intense research to improve their mechanical properties, the development of titanium alloys and later nickel super-alloys for turbine blades of air-breathing engines, the use of advanced composite materials for structural applications, etc.

Historically, much research has been devoted to the characterization of the mechanical properties of aerospace materials and to the development of techniques to produce components with tailored properties. On the contrary, the fact that metals exhibit viscoelastic behaviour under certain ambient and loading conditions has often been overlooked. Nevertheless, it is important to study the viscoelastic response of metals, and to comprehend the underlying physics of this phenomenon, in view of new potential applications and to better predict their performances in applications where they work under dynamic loads.

Fatigue, for instance, is a consequence of microstructural changes induced in a material under repeated loading, while the viscoelastic behaviour is intimately linked to the microstructure [1]. Accordingly, the characterization of the viscoelastic response of a material offers an alternative method for analyzing its microstructure and fatigue behaviour. In addition, it enables a deeper understanding of other technologically essential properties, like damping and yielding [1].

AlZnMgCu alloys have been chosen for this research because they feature excellent mechanical properties [2] and are suitable to a number of industrial applications, especially in the aerospace sector and transport industry. For instance, these alloys are widely used in aircraft skin panels, especially in military aircraft [3, 4], but also in commercial civil aviation aircrafts [5].

The proposed PhD is aimed at the identification, characterization and modelization, whenever possible, of the effects of temperature, frequency of dynamic loading, microstructure and phase transformations on the viscoelastic behaviour of AlZnMgCu alloys and the mechanical relaxation processes taking place. Ultimately, this research pursues to characterize the relation between the viscoelastic response of AlZnMgCu alloys under given operational conditions and their fatigue behaviour, which is of remarkable importance for the structural applications of these alloys.

This document consists of five chapters, being the first one this introduction. In Chapter 2, the state of the art on the viscoelastic properties of AlZnMgCu alloys and other topics related to the PhD proposal is presented. Chapter 3 deals with the definition of the objectives of the thesis proposal and the methodology and experimental techniques to be used. Next, the thesis current status, future work, tentative calendar, funding and publications related to this work are shown in Chapter 4. Finally, Chapter 5 concludes the PhD proposal with the summary.

2 STATE OF THE ART

In this chapter, the state of the art on the viscoelastic properties of AlZnMgCu alloys and other topics related to the PhD proposal is reviewed. First of all, the essentials of viscoelasticity are explained. Next, the influence of the microstructure on the viscoelastic properties and mechanical relaxation processes is briefly reviewed. The following section deals with the precipitation path of the target alloys. Finally, information is presented regarding the modelization of the various phase transformations that characterize the precipitation sequences of these AlZnMgCu alloys.

2.1 VISCOELASTICITY

Viscoelasticity is a property of materials that exhibit time-dependent strain [6]. On one hand, a perfectly viscous material exhibits stress proportional to strain rate. On the other hand, for perfectly elastic materials stress is proportional to strain and the proportionality constant is the Young's (or elastic) modulus. Viscoelastic materials feature intermediate characteristics between purely elastic and purely viscous behaviour, i.e. they show both viscous and elastic behaviour when undergoing deformation.

Whereas elasticity usually involves the stretching of atomic bonds (atomic displacements) along specific crystallographic planes in crystalline solids, viscosity and viscoelasticity involve relaxations associated to diffusion, a flow mechanism consisting in a continuous displacement with time of atoms or molecules within the material, enabling atomic rearrangements or cooperative motion of atomic groups [1, 7, 8]. The viscous flow results in frictional energy loss appearing as heat. Materials may exhibit viscoelastic relaxations in response to mechanical, electrical or temperature perturbations. The relaxation processes are then manifested by a transient response of physical or thermodynamic properties (e.g. enthalpy, volume, strain or stress) and are associated to the energy dissipation [7].

Nonetheless, to characterize the viscoelastic behaviour of a material, samples are usually excited dynamically under controlled temperature, frequency and amplitude of the loading, and the strain-stress behaviour is recorded. For instance, they are often strained or stressed sinusoidally with a Dynamic-Mechanical Analyzer (DMA). For an ideal elastic material, stress and strain are in phase, and the energy lost as heat per cycle is null. For an ideal viscous material, stress and strain are 90º out of phase. In reality, viscoelastic behaviour is more common. Thus, for most of the materials there is usually an intermediate phase lag between stress and strain (i.e. they are out of phase) and a certain amount of frictional energy loss (see Fig. 1). Polymers, polymer solutions and dispersions, metals and amorphous materials (organic and inorganic) are examples of materials that exhibit viscoelastic behaviour.

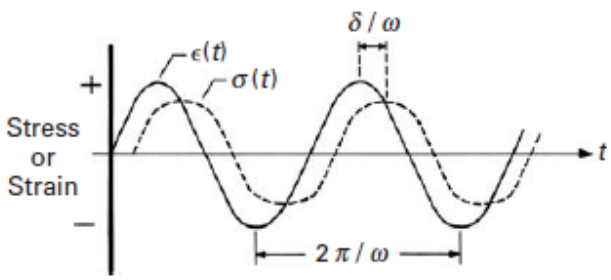

Fig. 1 Viscoelastic response of a material with phase lag between stress and strain [6].

The parameters utilized for the characterization of the viscoelastic behaviour are usually the two components of the tensile modulus and the loss tangent. First, the storage modulus *E'*, which is a measure of the stored (deformation) energy, corresponding to the elastic (real) component of the tensile modulus. Second, the loss modulus *E''*, which corresponds to the viscous (complex or plastic) component, represents the frictional energy loss (internal friction or energy dissipated as heat) during the relaxation processes. Finally, the loss tangent or tan δ (see Fig. 2) is the ratio of energy loss to energy stored, i.e. the ratio loss modulus to storage modulus.

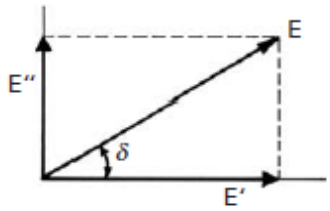

Fig. 2 Relationship between the storage modulus, the loss modulus and the loss tangent [6].

2.2 INFLUENCE OF MICROSTRUCTURE ON VISCOELASTIC BEHAVIOUR

As mentioned before, the mechanical properties of materials are intimately linked to their microstructure [9, 10]. Thereby, the microstructure and microstructural transformations are reflected on the viscoelastic behaviour. Particularly, the viscoelastic response in crystalline materials may involve different types of mechanical relaxation processes. The physical origin for these relaxations is the mechanism of diffusion, and they are related to a series of internal variables in crystalline solids that depend on stress in a time-dependent manner [1].

The types of mechanical relaxation processes determined by the microstructure which fall within the scope of this work are:

- Point-defect relaxations.
- Relaxations related to dislocations.
- Relaxations related to grain boundaries.
- Relaxations related to phase transformations.

2.2.1 Point-defect relaxations

In this case, the existence of the above mentioned internal variables is associated to the presence on diverse crystallographic sites of the microstructure of a class of crystal imperfections named point defects. The simplest point defects, the so-called elementary point defects, are:

- Vacancy: results from removing an atom from the crystal.
- Substitutional atom: results from substituting an atom with an atom of different species.
- Interstitial atom: results from bringing an extra atom (of the same or different species) into a position which is not a regular lattice site.

Furthermore, composite defects or defect complexes are produced by a combination of two or more elementary point defects.

The presence of a point defect in the crystal causes local elastic distortions. The mechanical relaxations associated to these defects arise due to the interactions between the distortion stress fields of the defects and the stress applied to the crystal [1].

Examples of mechanical relaxation processes involving point defects are, for instance, the migration of solute species and the migration of vacancies or solute-vacancy pairs, and more particular cases like the Snoek relaxation, i.e. impurity interstitials in body-centered cubic (bcc) metals lattice, and the Zener relaxation [1].

2.2.2 Relaxations associated to dislocations

Relaxation effects (i.e. the viscoelastic response) are associated to the presence and displacement of microstructural line imperfections named dislocations. Dislocations are linear or one-dimensional defects around which some atoms are misaligned [11].

Particularly, relaxation phenomena are associated to the lag between the motion of dislocations and the applied stress. This might occur when obstacles or potential barriers (e.g. point defects) impede the displacement of the dislocations [1].

In almost all cases, the material must be in a cold-worked or deformed state for these relaxation effects due to dislocation motion alone to occur. Nevertheless, internal friction due to point defects alone or due to dislocation motion interacting with point defects might also occur in deformed state materials, since their defect structure is highly complex.

Examples of mechanical relaxation processes, observable as internal friction peaks, associated to motion of dislocations are, for instance, the Bordoni peak in face-centered cubic (fcc) metals, attributed to dislocations alone, or the Hasiguti peaks and the Snoek-Köster peak, attributed to dislocation motion in combination with point defects [1].

2.2.3 Relaxations associated to grain boundaries

It is well accepted also that relaxation processes related to grain boundaries in metals and alloys do occur. The grain boundaries are the microstructural interfaces that separate one crystal or grain from another in a polycrystalline material.

In this case, the viscoelastic effects arise due to the occurrence of sliding at the boundary between adjacent grains. Schematically, these processes start, upon application of stress, with the sliding of a grain over the adjacent one due to the shear stress that initially acts across their boundary. Thereby, shear stress is gradually reduced and opposing stresses build up at the end of the boundary and into other adjacent grains. This process ends when the shear stress reaches zero across most of the boundary and the grain corners sustain most of the total shearing force [1].

2.2.4 Relaxations associated to phase transformations

Finally, relaxation effects might be related to phase transformations. A phase transformation is a process by which a material undergoes a change from one phase or mixture of phases to another. This process might involve a modification of the crystal structure or the state of order of the crystal. Examples of phase transformations are allotropic, eutectoid, order-disorder, ferromagnetic and ferroelectric transformations. The latter three are changes of atomic order, magnetic order and dipolar order respectively [1].

The internal state of a material close to a transformation might be described by one or more internal order variables. Viscoelastic behaviour has been reported in materials close to the transition critical temperature that is attributed to changes in the order variables caused by stress. Another example of relaxation effects associated to phase transformations is the influential role that stress might play in changing the state of two-phase materials in which the formation mechanism is nucleation and growth.

2.3 PRECIPITATION PATH OF AlZnMgCu ALLOYS

Age hardening is based on the formation of intermetallic products from the decomposition of a metastable super-saturated solid solution (SSS), which is obtained by solution treatment and quenching. The interaction between the decomposition products and the dislocations is the main responsible for the hardening [2]. That is, the particular precipitation (or decomposition) path and phase transformations (which in turn depend on the alloy composition and the ageing parameters) determine the microstructure, and hence the material properties, too.

This is the reason why important research efforts have been focused on the investigation of the precipitation process (transformation sequence during ageing) in metals. This research has been particularly intense in AlZnMg alloys (series 7000) [12] and in AlCuMg alloys (series 2000) because these families are highly suitable to a number of industrial applications, especially in the aerospace sector and transport industry. Their commercial and industrial importance stems from their excellent mechanical properties.

Two important alloys are chosen as key representatives of their respective families for the scope of this research: aluminium alloy (AA) 7075 and AA 2024. These alloys have been selected due to their widespread use in aircraft skin panels, especially in military aircraft [3, 4], but also in commercial civil aviation aircrafts [5].

2.3.1 Precipitation path of AA 7075

For the alloys of the family AlZnMg, it is generally accepted that the age-hardening mechanism is essentially based on the following precipitation path or ageing sequence [12-15]:

- α_{SSS} – GPZ I – GPZ II – η’ – η

where GPZ are the Zn/Mg solute-rich coherent clusters named Guinier-Preston Zones, η’ the semi-coherent (metastable) hexagonal $MgZn_2$ phase and η the incoherent stable (equilibrium) hexagonal $MgZn_2$ phase.

2.3.2 Precipitation path of AA 2024

For the alloys of the family AlCuMg, it is generally accepted that the age-hardening mechanism is essentially based on two different precipitation paths (or ageing sequences) [2, 16-19]

- α_{SSS} – GPZ – θ'' – θ' – θ
- α_{SSS} – GPBZ – (S’’) – S' – S

where GPZ are the Cu solute-rich coherent clusters named Guinier-Preston Zones, θ'' and θ' the semi-coherent (metastable) Al_2Cu phases, θ the incoherent stable (equilibrium) Al_2Cu phase, GPBZ

the Cu/Mg Guinier-Preston-Bagariastkij zones, S'' and S' the semi-coherent (metastable) Al_2CuMg phases and S the incoherent stable (equilibrium) Al_2CuMg phase [2]. The existence of an intermediate phase S'' between GPBZ and S' is still a controversial issue at present day.

In the case of AlZnMgCu alloys, apart from the above mentioned, a third precipitation sequence is present too [17], which was already addressed in the previous section:

- α_{SSS} – GPZ I – GPZ II – η' – η

There are no indications of possible interactions between these three different sequences which seem to develop independently [17].

2.4 KINETICS OF PHASE TRANSFORMATIONS

In phase transformations of materials, the following mechanisms usually appear interrelated: thermodynamic effects, kinetic effects and mass transport [20]. In this section we introduce some issues related to the kinetics of phase transformations that are of significant interest for the scope of this work.

2.4.1 Modelling the phase transformation kinetics of AlZnMgCu alloys

Significant research has been devoted to the study and modelization of the phase transformations that characterize the precipitation sequences of AlZnMgCu alloys and other materials. In particular, several types of rate equations have been proposed that establish the time-evolution of the transformed fraction during the corresponding transformation. First, the Johnson-Mehl-Avrami model, which is commonly used to describe the kinetics of nucleation and growth transformations, where the formation of a new phase typically follows a sigmoidal curve [20, 21], such as:

$$Y(t) = 1 - \exp(-(t/\tau)^n) \qquad \textbf{Eq. 1}$$

where Y is the transformed fraction, t is the time, τ the characteristic transformation time and n is the Avrami exponent or index. Both τ and n are independent of time. The transformation time is determined by the activation energy and the transformation temperature, and thus will decrease as the transformation temperature increases. The Avrami exponent depends on the nature of the transformation. On one hand, it allows the determination of whether the atom motion during the transformation is of short-range type (case of interface controlled transformations) or of long-range type (case of diffusion controlled transformations). On the other hand, the Avrami exponent also differs depending on whether nucleation only occurs at the beginning of the transformation (case of site-saturated nucleation) or whether new nuclei appear in untransformed regions along the transformation (case of continuous nucleation). Namely, in 3D diffusion controlled transformations with site-saturated nucleation, the Avrami exponent has usually values close to 1.5. Finally, it is noteworthy that the Avrami model relates only to kinetics and stems simply from geometrical considerations (i.e. the rate of occupation of the space by the new phase), and its application does not require any assumption or consideration regarding the thermodynamics of the problem.

For example, from Differential Isothermal Calorimetry (DIC) scans, Smith obtained information on the kinetics of some phase transformations of AA 2124 using a 2-exponential fit and a rate-averaged time constant, but for GPZ formation, he analyzed the kinetics using the Johnson-Mehl-Avrami model [16]. Smith also established criteria for choosing the most suited models to analyze DIC data. For instance, he states that the 2-exponential fit is applicable when two distinct processes

contribute to precipitation, while the rate-averaged time constant is appropriate when only one process is dominant [16].

From Differential Scanning Calorimetry (DSC) data, Papazian calculated the GPZ dissolution processes (i.e. transformed fraction *Y* vs. temperature *T* curves) for AA 2219 and A 7075 using a first order diffusion expression, Eq. 2, and a 3D volume diffusion limited rate expression, Eq. 3 [22]:

$$-\ln(1-Y) = \frac{k_0 E_A}{K\phi}\int_{\frac{E_A}{KT}}^{\infty}\frac{e^{-x}}{x^2}dx \qquad \textbf{Eq. 2}$$

$$\left[1-(1-Y)^{1/3}\right]^2 = \frac{k_0 E_A}{K\phi}\int_{\frac{E_A}{KT}}^{\infty}\frac{e^{-x}}{x^2}dx \qquad \textbf{Eq. 3}$$

where k_0 is the frequency factor, E_A the activation energy, K the Boltzmann constant, Φ the DSC heating rate and T the temperature. Papazian's results using these models were:

- For AA 2219 aged at low temperature: In this case, the analysis of the kinetically dominated reaction peaks in the DSC thermograms and their dependence on heating rate and particle size led the author to conclude that GPZ dissolution is best described by the latter relationship i.e. the 3D volume diffusion limited rate expression. The author supports this conclusion on several arguments. First, this law was originally developed to describe the kinetics of solid state reactions in powders [23]. Thus, there is some similarity between the physical basis for the law and the diffusion controlled dissolution of GPZ. Second, the activation energy for GPZ dissolution is precisely equal to the activation energy for the chemical inter-diffusion in AlCu systems. Finally, the first order relationship has little physical justification in solid state reactions and the required value for the activation energy cannot be simply related to a physical process in the studied system.
- For AA 7075 aged at low temperature, i.e. aged 6 months at room temperature (RT), and AA 7075-T651: As an important remark, the value of the activation energy for the 3D volume diffusion limited rate expression was chosen from the activation energy for self-diffusion of Zn in the AlZn system, interpolated to the composition of AA 7075 [24]. Although both expressions fit the experimental data reasonably well, Papazian concludes that the GPZ dissolution in AA 7075 is also best described by the 3D volume diffusion limited rate expression, again because of the physical basis of this diffusion controlled rate expression and the appropriateness of the activation energy.

Papazian also concluded that the rate of formation of θ' is best described by an Avrami expression with *n* 1.1 [22]. Values of *n* between 1 and 1.5 are typical of the growth of particles of appreciable initial nucleus size [21]. This value of *n* and the insensitivity of θ' formation to deformation indicates that nucleation of θ' is not the overall rate controlling step. On the other hand, for η' phase formation and growth of as-quenched specimens and aged specimens, the Avrami index for the transformation has been inferred to be about 2.3-2.8 (+/-20%) [25], which may correspond to a diffusion controlled transformation with continuous nucleation.

Alternative expressions for modelling the transformation kinetics are reported in the literature. For instance, assuming that the particular phase transformation is a temperature- or thermally-activated process, the concentration of the species may follow the Arrhenius behaviour. In this case, the transformation rate equation is [19, 21]:

$$\frac{dY}{dt} = f(Y)k_0 \exp\left(-\frac{E_A}{KT}\right) \qquad \textbf{Eq. 4}$$

where k_0 is the pre-exponential or frequency factor. In support of a statement at the beginning of this section, Jena states that precipitation reactions that occur by nucleation and growth yield sigmoidal behaviour and are best described either by the Johnson-Mehl-Avrami model, Eq. 1, or by Eq. 4 with:

$$f(Y) = Y^r (1 - Y)^m \qquad \textbf{Eq. 5}$$

where coefficients *r* and *m* are constants [19]. In this latter paper, Jena reports also which values of *r*, *m*, k_0 and E_A provide the best fit to experimental data for several phase transformations of the AlCuMg alloys precipitation sequence, namely GPBZ precipitation, GPZ dissolution, dissolution of GPBZ-dislocation complexes and S' precipitation. The latter transformation satisfies also the Johnson-Mehl-Avrami equation (*n* being 1). Finally, say that the model by Jena combines kinetics and thermodynamics considerations and that no explanation is given by the author for its physical basis.

2.4.2 Activation energies for phase transformations of AA 7075

A summary of the values found in the literature for the activation energies of the phase transformations involved in the precipitation path (ageing sequence) of the AA 7075 is presented in this section. For some of its transformation processes no information was found in literature regarding their kinetics and/or activation energies. The causes for the absence of literature reporting about these issues are three, to the author's knowledge:

- The calculation of the activation energy is not possible due to a particular reason, e.g. in DSC scans, when the peak corresponding to the particular phase transformation is overlapped [22].
- The corresponding phase transformation is thermodynamically controlled (i.e. it is controlled by temperature dependent thermodynamic equilibrium), so the kinetic factors are not important [19].
- No researcher has analyzed the kinetics of the particular transformation for AA 7075 (or for AA 2024), to the author's knowledge. In these cases, as indicated below, information on activation energies of other AlZnMg (or AlCuMg) alloys has been depicted instead, whenever found.

Summary of findings on activation energies for AA 7075:

1. GPZ formation:
    a. For Zergal 4 (commercial AlZnMgCu alloy, with composition Al–6.0 wt% Zn–2.0 wt% Mg–1.0 wt% Cu) the activation energy for the reconstruction of GPZ is in the range 0.59-0.67 eV per atom [15].
    b. For AlZnMgZr alloy the (isothermal) activation energy is reported to be 0.35 eV per atom when using a method based on hot micro-hardness data, and 0.75 eV per atom when using data from variable heating rate DSC scans, analyzed by the Kissinger method [25]. In this paper, other values are reported too from previous DSC studies: 0.41 eV per atom [26], 0.67 eV per atom [27], and 0.65-1.08 eV per atom.

2. GPZ dissolution[3]:
    a. Activation energies are [28]:
        i. For AA 7075-T6: 135000 J/mole (1.40 eV per atom).
        ii. For AA 7075-T6 followed by Retrogression and Re-ageing (RRA): 145000 J/mole (1.50 eV per atom).
        iii. For AA 7075-T85: 150000 J/mole (1.55 eV per atom).
    b. For Zergal 4 (commercial AlZnMgCu alloy, with composition Al–6.0 wt% Zn–2.0 wt% Mg–1.0 wt% Cu), for GPZ dissolution and simultaneous η' formation, i.e. transformation GPZ-η', the activation energy is 0.32 eV per atom [15, 29].
    c. For AA 7075 aged 6 months at RT and for AA 7075-T651, the activation energies using a first order diffusion expression and a 3D volume diffusion limited rate expression were 75000 J/mole (0.78 eV per atom) and 123000 J/mole (1.27 eV per atom), respectively [22].
    d. Activation energies are [25, 30]:
        i. For AA 7075 naturally aged: 0.93-0.99 eV per atom.
        ii. For AA 7075-T6: 1.23 eV per atom.
        iii. For AA 7091: 0.99 eV per atom.
    e. For AlZnMgZr alloy the (isothermal) activation energy is reported to be 0.92 eV per atom when using data from variable heating rate DSC scans, analyzed by the Kissinger method [25].
3. η' formation and coarsening (or growth):
    a. For AlZnMgZr alloy the activation energy for η' formation and growth for as-quenched specimens and aged specimens is reported to be: 0.57, 0.59 and 0.62 eV per atom [25]. These values compare well with the activation energy for Mg migration in AlZnMg system (0.60 eV per atom) and with the activation energy for Zn–vacancy pair migration in AlMg (0.40-0.55 eV per atom).
    b. It is difficult to find references that report the activation energy for this phase transformation. The reason might be that, although it is kinetically controlled, the precipitation of η' is not good for kinetics analysis since its peak in DSC thermograms appears overlapped with those of other phase transformations, as occurs for instance in DSC curves of AA 7075 [22].
4. η' dissolution: No references have been found that report the activation energy for this phase transformation. The reason might be the same as for η' formation [22].
5. η formation and coarsening (or growth): No references have been found that report the activation energy for this phase transformation. The reason might be the same as for η' formation and dissolution [22].
6. η dissolution: No references have been found that report the activation energy for this phase transformation, the reason being probably that η dissolution is controlled by thermodynamics (temperature dependent thermodynamic equilibrium), so the kinetic factors are not important in this case [19, 22].

Table 1 summarizes representative values of the activation energy for the various phase transformations involved in the precipitation sequence of AA 7075.

[3] The activation energy for the GPZ formation and for the GPZ dissolution should not necessarily be equal. In the GPZ formation process there is an excess of solute while in the dissolution process there is a lack of solute. Nevertheless, both processes are related to atomic mobility of the same species, thus their activation energies should be of a similar order of magnitude.

Table 1 Activation energy for phase transformations of the precipitation sequence of AA 7075.

Phase transformation	Activation energy [eV/atom]	References	Observations
GPZ formation	0.59-0.67	[15]	Zergal 4 (commercial AlZnMgCu)
	0.35-1.08	[25]	AlZnMgZr alloy
GPZ dissolution	1.40	[28]	AA 7075-T6
	1.27	[22]	AA 7075 aged 6 months at RT
	1.23	[30]	AA 7075-T6
η' formation and coarsening	0.57-0.62	[25]	AlZnMgZr alloy
η' dissolution	-	[22]	Not good for kinetics analysis
η formation and coarsening	-	[22]	Not good for kinetics analysis
η dissolution	-	[19, 22]	Thermodynamically controlled

2.4.3 Activation energies for phase transformations of AA 2024

Analogously, here follows the summary of findings on activation energies for AA 2024:

1. GPZ or GPBZ formation:
    a. For GPBZ formation in AlCuMg alloy the activation energy is 52300-55600 J/mole (0.54-0.58 eV per atom) or 64000 J/mole (0.66 eV per atom) by resistivity measurements [19].
    b. For AA 2124, the activation energy is reported to be 73300 J/mole (0.76 eV per atom) when using DSC data, and 76200 J/mole (0.79 eV per atom) when analyzing DIC data [16]. Hence, activation energies from DSC and DIC agree fairly well.
2. GPZ or GPBZ dissolution:
    a. For GPBZ dissolution in AlCuMg alloy the activation energy is 123900 J/mole (1.28 eV per atom) [19].
    b. For AA 2219-T31 and AA 2219 aged at low temperature, the activation energies using a first order diffusion expression and a 3D volume diffusion limited rate expression were 79500 J/mole (0.82 eV per atom) and 126000 J/mole (1.31 eV per atom), respectively [22].
    c. For AA 2124, the activation energy is 159900 J/mole (1.66 eV per atom) [16].
3. θ" formation and coarsening (or growth):
    a. For AlCu alloys (AA 2024 and AA 2618) the activation energy is 129000 J/mole (1.34 eV per atom) [18].
    b. For AA 2124, the activation energy is reported to be 131000 J/mole (1.36 eV per atom) when using DSC data, and 128000 J/mole (1.33 eV per atom) when analyzing DIC data [16].
4. θ" dissolution: No references have been found that report the activation energy for this phase transformation.
5. θ' formation and coarsening (or growth):
    a. For AlCu alloys (AA 2024 and AA 2618) the activation energy is 117000 J/mole (1.21 eV per atom) [18, 31].
    b. For AA 2219-T31 and AA 2219-T42, the θ' formation process (i.e. transformed fraction *Y* vs. temperature *T* curves) was calculated using an Avrami expression, resulting in an activation energy of 117000 J/mole (1.21 eV per atom) [22]. The author states that the formation rate of θ' is best described by an Avrami model.

   c. For AA 2124, the activation energy is reported to be 113900 J/mole (1.18 eV per atom) when using DSC data, and 128000 J/mole (1.33 eV per atom) when analyzing DIC data [16].
   d. For AlCu alloys, values of 0.75 and 1.10±0.10 eV per atom were also reported [32]. These differences are explained in terms of mobility of dissolved atoms (related to vacancy concentration), interfacial energy and direction of growth (normal or perpendicular to θ'-phase plate).
6. θ' dissolution: No references have been found that report the activation energy for this phase transformation. The reason might be that, although it is dominated by kinetics, the dissolution of θ' is not good for kinetics analysis since its peak in DSC thermograms appears overlapped with those of other phase transformations, as occurs for instance in DSC curves of AA 2219 [22].
7. θ formation and coarsening (or growth): No references have been found that report the activation energy for this phase transformation. The reason might be the same as for θ' dissolution [22].
8. θ dissolution: No references have been found that report the activation energy for this phase transformation, the reason being probably that θ dissolution is controlled by thermodynamics (temperature dependent thermodynamic equilibrium), so the kinetic factors are not important in this case [19, 22].
9. S' formation and coarsening (or growth):
   a. For AlCuMg alloys (AA 2024 and AA 2618) the activation energy is 129900 J/mole (1.35 eV per atom) [18, 19], close to that for diffusion of solute atoms and consistent with other reported values [22].
10. S' dissolution: No references have been found that report the activation energy for this phase transformation, the reason being probably that S' dissolution is controlled by thermodynamics (temperature dependent thermodynamic equilibrium), so the kinetic factors are not important in this case [19].
11. S formation and coarsening (or growth): No references have been found that report the activation energy for this phase transformation.
12. S dissolution: No references have been found that report the activation energy for this phase transformation.

Table 2 summarizes representative values of the activation energy for the various phase transformations involved in the precipitation sequence of AA 2024.

Table 2 Activation energy for phase transformations of the precipitation sequence of AA 2024.

Phase transformation	Activation energy [eV/atom]	References	Observations
GPZ/GPBZ formation	0.54-0.66	[19]	AlCuMg alloy
	0.76 and 0.79	[16]	AA 2124
GPZ/GPBZ dissolution	1.28	[19]	AlCuMg alloy
	1.31	[22]	AA 2219-T31 and AA 2219
	1.66	[16]	AA 2124
θ” formation and coarsening	1.34	[18]	AA 2024 and AA 2618
	1.33 and 1.36	[16]	AA 2124
θ” dissolution	-	-	No references have been found
θ’ formation and coarsening	1.21	[18]	AA 2024 and AA 2618
	1.21	[22]	AA 2219-T31 and AA 2219
	1.18 and 1.33	[16]	AA 2124
	0.75 and 1.10±0.10	[32]	
θ’ dissolution	-	[22]	Not good for kinetics analysis
θ formation and coarsening	-	[22]	Not good for kinetics analysis
θ dissolution	-	[19, 22]	Thermodynamically controlled
S’ formation and coarsening	1.35	[18]	AA 2024 and AA 2618
S’ dissolution	-	[19]	Thermodynamically controlled
S formation and coarsening	-	-	No references have been found
S dissolution	-	-	No references have been found

3 DEFINITION OF THE PhD THESIS

In this chapter, the objectives of the PhD thesis are listed first. Next, the methodologies that are being applied in this research work to meet the mentioned objectives are briefly reviewed. In particular, the experimental methods are depicted firstly and, finally, the procedure followed for the data analysis and modelling is explained.

3.1 OBJECTIVES OF THE PhD THESIS

The proposed PhD is aimed at:

- Description of the viscoelastic behaviour of AlZnMgCu alloys:
    - Identification and characterization of the effects of temperature and dynamic loading frequency on the viscoelastic response of AlZnMgCu alloys:
        - Discussion of the effects on the storage modulus.
        - Discussion of the effects on the loss modulus.
        - Discussion of the effects on the loss tangent.
    - Identification and characterization of the influence of the microstructure and phase transformations on the viscoelastic response of AlZnMgCu alloys:
        - Modelization of the effects of formation and dissolution of the several phases involved in the precipitation paths of AlZnMg and AlCuMg alloys.
        - Determination of the influence of grain size.
    - Identification and characterization of the relaxation processes involved in the viscoelastic response of AlZnMgCu alloys:
        - Determination of the types of relaxations responsible for the viscoelasticity of these alloys: point-defect relaxations, relaxations related to dislocations, to grain boundaries or to phase transformations. Role of dislocations on the viscoelastic response.
        - Determination of the internal variables associated to theses processes.
        - Calculation of the activation energy, relaxation magnitude and relaxation time of the processes involved, if possible and/or applicable.
- Relationship between the viscoelastic behaviour and fatigue in AlZnMgCu alloys:
    - Characterization of the viscoelastic response of AlZnMgCu alloys under typical operational conditions.
    - Determination of the influence of temperature and dynamic loading frequency on the fatigue response.
    - Role of dislocations on the fatigue response. Is there a connection with the role of dislocations on viscoelastic response?
    - Determination of the influence of the viscoelastic behaviour in the fatigue response of AlZnMgCu alloys in structural applications. Can the latter be predicted?

3.2 METHODOLOGY

3.2.1 Experimental methods

The experimental techniques that have been used so far, or that will be used in this research are:

- **Differential Scanning Calorimeter (DSC):**
  The DSC measures the energy necessary to establish a nearly zero temperature difference between a material and an inert reference, as the two specimens are subjected to identical temperature regimes in an environment heated or cooled at a controlled rate. Essentially, there are two types of DSC systems [33]:
  - Power compensation DSC: In this case, the temperatures of the sample and the reference are controlled independently using separate, identical furnaces. The temperatures are made identical by varying the power input to the furnaces. The energy required is a measure of the enthalpy or heat capacity changes in the sample relative to the reference.
  - Heat-flux DSC: In this case, the sample and reference are connected by a low resistance heat flow path (a metal disc). The assembly is enclosed in a single furnace. Enthalpy or heat capacity changes in the sample cause a difference in its temperature relative to the reference. The temperature difference is recorded and related to enthalpy change in the sample using calibration experiments.

- **Dynamic-Mechanical Analyzer (DMA):**
  The DMA is commonly used to measure the viscoelastic response of materials. This equipment applies a mechanical excitation of selected frequency and amplitude under controlled temperature conditions, and records displacements and stiffness. This allows the evaluation and characterization of intrinsic and extrinsic mechanical properties of the material, namely the viscoelastic behaviour (e.g. the storage modulus *E'*, the loss modulus *E"* and the loss tangent) and the creep response.

- **High Resolution Transmission Electron Microscope (HRTEM):**
  The HRTEM is an imaging mode of the TEM (see below) that allows the imaging of the crystallographic structure of a sample at an atomic scale [34].

- **Micro-hardness tester:**
  The hardness testers measure the hardness of materials, i.e. their resistance to localized plastic (irreversible) deformation [11]. The tester might measure the hardness in one or more of the existing scales: the Brinell, Rockwell or Vickers scales. Thus, the reading is named Brinell hardness (HB), Rockwell hardness (HR) or Vickers hardness (HV), respectively. In all these techniques, an indenter is stabbed in the surface of the material upon application of a given load. After the load is released, the hardness is calculated from either the measure of the depth of penetration or the measure of a characteristic dimension of the impression or print.

- **Transmission Electron Microscope (TEM):**
  TEM is a technique which operates on the same basic principles as the light microscopy but which uses a beam of electrons instead of light. The electron beam is transmitted through a very thin specimen and, after the interaction of the electron beam with the sample, the image is formed onto, for instance, a fluorescent screen or a layer of photographic film, or is detected by a sensor like a Charge-Coupled Device (CCD) camera. A TEM is capable of resolving objects at a significantly higher resolution than light microscopes, thanks to the much lower De Broglie wavelength of electrons respect to light. At lower magnifications, the contrast observed in TEM images is due to differences in the absorption of electrons in the

specimen which arise due to differences in the thickness and composition of the material. At higher magnifications, wave interactions modulate the intensity of the image and analysis of observed images is required [35].

- **Universal Testing Machine (UTM):**
  The UTM is capable of performing traction, compression and flexure tests on samples. These tests allow the determination of a number of mechanical properties of the materials. For instance, stress-strain curves can be obtained, and thanks to the acquired data, the following parameters can be calculated: the elastic modulus, yield stress, Ultimate Tensile Stress (UTS), ductility, resilience modulus, toughness, etc.

- **X-Ray Diffraction (XRD):**
  XRD is a non-destructive technique that is based on the observation of the scattered intensity of an X-ray beam after its interaction with the sample, as a function of the incident and scattered angle, the polarization and the wavelength or energy. The result of the interaction of the X-ray beam with a crystalline material or phase is a diffraction pattern. The key point is that a given substance always gives the same pattern, and that, in a mixture of substances, each produces its pattern independently of the others. The XRD is able to provide information about the chemical composition, the crystallographic structure (e.g. identification of polycrystalline phases) and the physical properties of materials [36, 37].

3.2.2 Data analysis and modelling

After having prepared the samples from the as-received plates of AA 7075-T6 and AA 2024-T3, and after having performed tests on them to measure experimentally the behaviour of the alloys, the procedures that we are following to analyse the data are summarized here.

First, our experimental data and other research in the literature are analyzed to identify which phenomena determine the behaviour of the alloys. In view of this information, empirical, semi-empirical and/or analytical macroscopic models, when appropriate, are proposed and/or taken from the literature. These models are integrated or solved (e.g. fitted) either analytically or numerically. For this purpose, we use commonly available computational tools and software packages.

The model results are then checked against the experimental data and other results in the literature to evaluate the goodness of the fit. The criteria to measure the latter is the value of the chi-square function, computed after the non-linear fit of the model to the test data. The quality of the fit is the main parameter to ascertain whether our physical interpretation of the phenomena governing the behaviour is correct. If necessary, the model is refined, rebuilt or disregarded.

Implementation of more sophisticated models, such as phase field modelling, may be considered if the fitting of experimental data to macroscopic models gives poor quality results.

4 PhD THESIS DEVELOPMENT

Once the thesis objectives and the state of the art have been reviewed, in this chapter the attention is focused on the thesis development. The current status of the research is depicted in the first section. In the following sections, the future work and the tentative calendar are presented. Finally, funding details and publications derived from this work are noted.

4.1 CURRENT STATUS

Next follows a summary of the research that has already been completed or that is close to completion. As much as it is possible, the tasks are presented in temporal order.

4.1.1 Research on the state of the art of key topics

Research on the state of the art of topics related to the thesis was the first task to be undertaken. Some of the results have already been presented in Chapter 2. During this process, emphasis was placed especially on the search on:

- Viscoelasticity and viscoelastic properties (e.g. creep behaviour) of aluminium alloys.
- Other mechanical properties and precipitation paths of aluminium alloys.
- Characteristics of phase transformations in aluminium alloys (e.g. kinetics).
- DSC and Transmission Electron Microscope (TEM) analyses of aluminium alloys.
- Parameters that affect the elastic constants, and particularly the Young's modulus and the storage and loss moduli.
- Time-Temperature Superposition (TTS) principle.
- Relationship between viscoelastic properties, temperature, frequency of dynamic loading, dislocations density and fatigue behaviour.

Searches in literature regarding these topics are planned to be performed periodically, in order to update the available information and state of the art within the framework of this thesis. This process will continue until the final delivery of the thesis.

4.1.2 Experimental results on viscoelastic response of AlZnMgCu alloys

A TA Instruments Q800 DMA has been used to measure the viscoelastic response of AlZnMgCu alloys. The tested specimens were rectangular plates of 60 mm in length, 8 to 15 mm in width and 2 mm in thickness. These samples were machine cut from sheet of as-received AA 7075-T6. The DMA was configured to sequentially apply dynamic loading with frequencies of 100, 30, 10, 3 and 1 Hz at different temperatures, from 35 to 375 ºC in step increments of 5 ºC. Some tests were set to reach higher temperatures, but results were disregarded as plastic deformations occurred for the applied stress levels. During the tests, the storage and loss moduli *E'* and *E"* were computed for each of the frequencies at each temperature step.

Figure 3 shows the storage modulus, i.e. the elastic (real) component of the tensile modulus, as a function of temperature for mechanical excitations of frequencies 100, 30, 10, 3 and 1 Hz, for AA 7075-T6. As a general trend, the storage modulus decreases initially for all the frequencies. The

slope becomes more pronounced at about 130-160 ºC, and an inflexion appears around 200-250 ºC. Finally, there is a local maximum around 300 ºC, after which the storage modulus decreases again. Another important observation is that the storage modulus depends more significantly on frequency at high temperatures, i.e. above 100 ºC, being almost insensitive to frequency below this temperature threshold. In addition, at high temperatures, the decrease in the storage modulus at low frequencies is larger than that at higher frequencies.

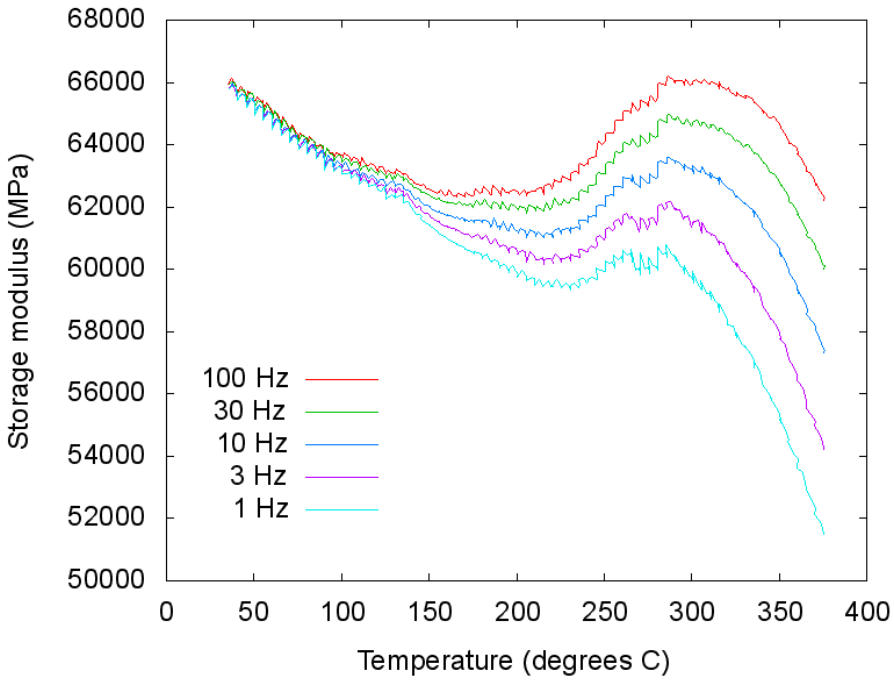

Fig. 3 Storage modulus *E'* vs. temperature *T* obtained by dynamic-mechanical tests with DMA on AA 7075-T6 at different frequencies.

The loss modulus, i.e. the viscous (complex) component of the tensile modulus, which accounts for the frictional energy dissipation during relaxation processes [1], is shown in Fig. 4. It exhibits no significant changes at low temperatures, but starts to increase at about 130-160 ºC. This reflects that more energy is dissipated through viscoelastic processes, i.e. internal friction, as temperature increases. It is worth to mention that for all of the tests the loss modulus increases monotonically: no peak is observed in the studied temperature range.

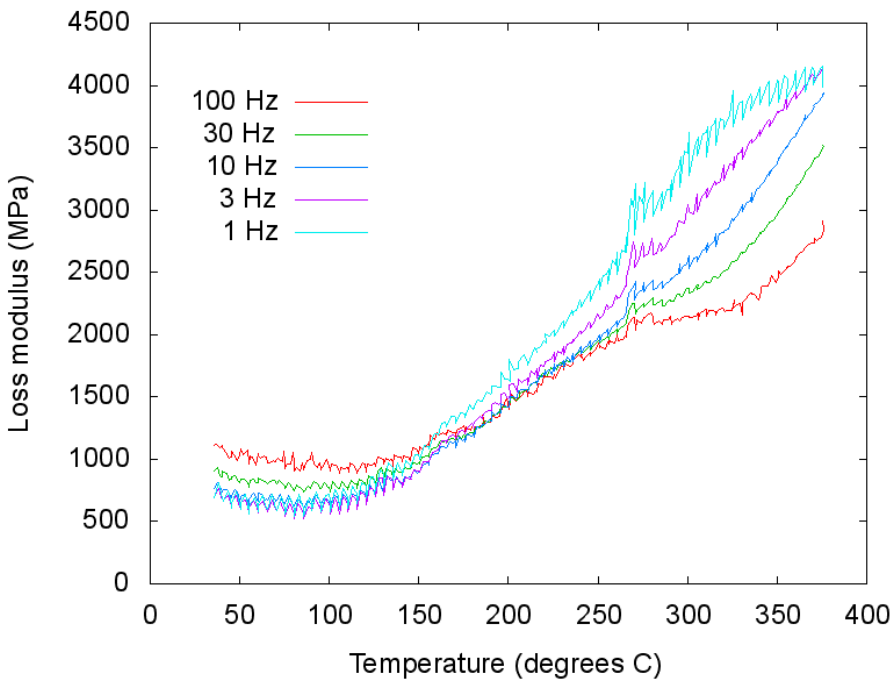

Fig. 4 Loss modulus *E"* vs. temperature *T* obtained by dynamic-mechanical tests with DMA on AA 7075-T6 at different frequencies.

4.1.3 Modelling of the storage modulus behaviour

It is clear from the experimental data that the viscoelastic response depends on temperature and the frequency of the mechanical excitation. Also, according to the available TEM and DSC data in literature [14, 22, 25, 28, 30], as well as studies on precipitation sequences and hardening mechanisms [13], it is expected that the mechanical response of the target alloy below 220 ºC is controlled by the presence and decomposition of GPZ. These clusters can be seen in Fig. 5 for an AlCuMg alloy after 2760 min of ageing at RT [2]. Accordingly, we proposed an analytical model for the evolution of the storage modulus *E'* as a function of temperature *T*, the frequency of the dynamic loading *f* and GPZ concentration, denoted as *C*:

$$E'(f,T) = E'_0(f) + E'_1(f)T + E'_2(f)C(T) \qquad \textbf{Eq. 6}$$

where E'_0 is the storage modulus at 0 K, E'_1 accounts for a linear decrease in the storage modulus with temperature due to thermal expansion (see Section 4.1.4 for details), and E'_2 reflects the contribution of GPZ to the storage modulus. These coefficients are determined by non-linear fit of the model to experimental data. The model is valid when the only significant microstructural transformation present is the GPZ dissolution, i.e. up to around 200 ºC.

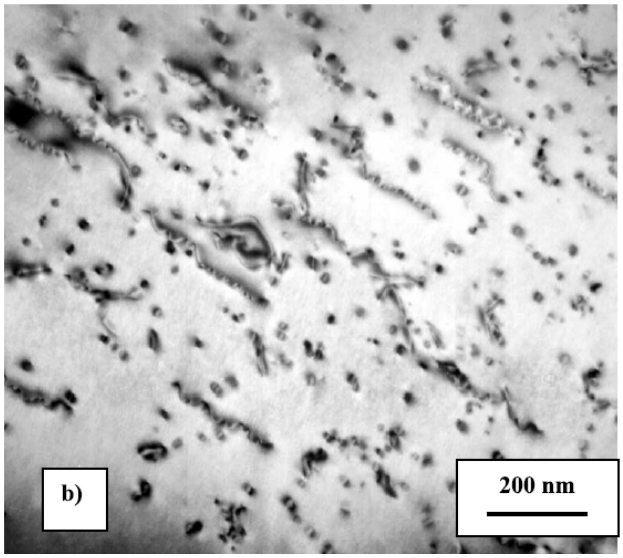

Fig. 5 TEM micrograph showing GPZ precipitates in an AlCuMg alloy after 2760 min of ageing at room temperature. Reproduced with permission from Abis *et al.* [2].

As mentioned before, being the GPZ dissolution a thermally-activated process, GPZ concentration may follow the Arrhenius behaviour. Thus, as proposed by Jena [19, 21], the transformation rate equation that best represents the GPZ dissolution is:

$$\frac{dC}{dt} = -Ck_0 \exp\left(-\frac{E_A}{KT}\right) \qquad \textbf{Eq. 7}$$

where k_0 is a pre-exponential coefficient and E_A the activation energy of the GPZ dissolution process (both are constants), and K is the Boltzmann constant. Nevertheless, as mentioned before too, alternative expressions for modeling GPZ dissolution rate are reported in the literature. Papazian used a 3D diffusion controlled rate expression, Eq. 3, and a first order diffusion rate expression, Eq. 2 [22], that we will call Papazian I and Papazian II from now on. The latter equations and Eq. 7 were all implemented in our model and cross-checked to ascertain which one provided a better fit to experimental data.

Numerical integration of the rate equation was performed by using a Runge-Kutta method inside the least-squares non-linear fitting of the storage modulus model to experimental data. This allows us to treat the pre-exponential coefficient and the activation energy as fitting parameters, in addition to coefficients E'_0, E'_1 and E'_2. The initial values used for the fitting procedures are directly taken or estimated from data available in the literature and are summarized in Table 3.

Table 3 Initial guess parameters for the integration of the transformation rate equation and the non-linear fitting of the proposed storage modulus model, Eq. 6, for the case of AA 7075-T6.

Parameter	Value	References
GPZ concentration, C	4.9 %	[12, 38-41]
Pre-exponential coefficient, k_0	1.0×10^{9} or 1.0×10^{10} s^{-1}	[1, 19]
Activation energy, E_A	1.32 eV/atom	[15, 22, 25, 28-30]
Coefficient E'_0	E' at RT	-
Coefficient E'_1	-1.5×10^{7} PaK^{-1}	[42-45]
Coefficient E'_2	5.0×10^{10}	-

An example of the experimental and numerical storage modulus at 100 Hz, plotted against temperature, is shown in Fig. 6. The computed evolution of GPZ concentration with temperature is shown in Fig. 7, together with the previous numerical values of storage modulus. As can be seen, the GPZ concentration exhibits a characteristic sigmoidal shape, provided the oscillations[4] in the plot are not taken into account.

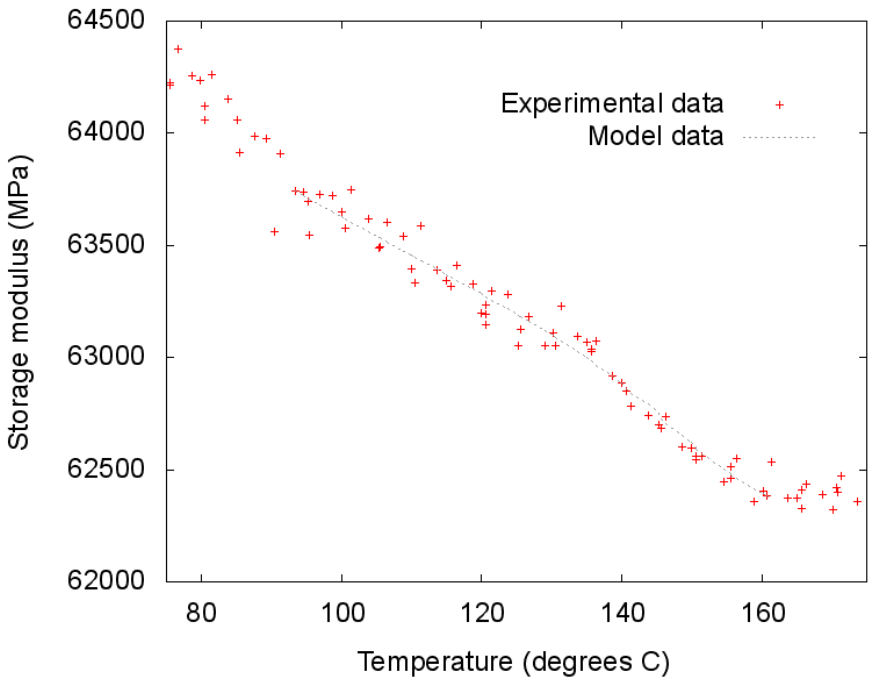

Fig. 6 Experimental and numerical results of storage modulus E' vs. temperature T, for AA 7075-T6, at a frequency of 100 Hz.

[4] These oscillations appear only for the computed GPZ concentration when using Jena's rate equation, Eq. 7, and not when using Papazian's rate equations, Eq. 2 and 3. The oscillations are not due to any kind of error or under-performance of the solver code. They originate simply because, for the integration of Eq. 7, it is necessary to input data on the evolution of temperature with time and, for this purpose, we utilized the recorded test temperature, which features steps with time. For Papazian's rate equations, this type of input is not necessary. Thereby, the computed GPZ concentration is in this case a smooth curve with no oscillations.

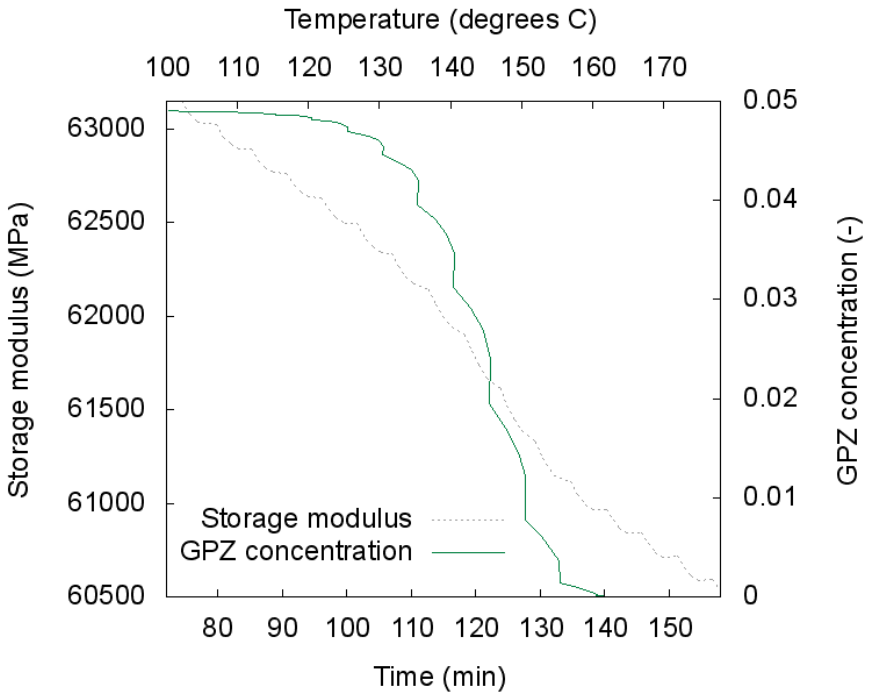

Fig. 7 Numerical results of storage modulus *E'* vs. time *t*, at a frequency of 100 Hz, and GPZ concentration *C* vs. temperature *T*. These data is for AA 7075-T6.

The physical quantities of interest, i.e. the pre-exponential coefficient and the activation energy of the GPZ dissolution process for Jena's and Papazian's rate equations, are listed in Table 4. The storage modulus coefficients E'_1 and E'_2 are displayed in Fig. 8. As will be commented in Section 4.2, the identification and characterization of patterns in the behavior of E'_1 and E'_2 with frequency is a planned task. At this point, no remarkable findings in regard to this issue can be presented here.

Table 4 Best-fit values obtained after integration of the considered models, for the case of AA 7075-T6.

Rate equation	Parameter	Average value	Standard deviation
Jena	Pre-exponential coefficient, k_0	1.15×10^9 s^{-1}	1.40×10^9
	Activation energy, E_A	1.16 eV/atom	0.08
Papazian I	Pre-exponential coefficient, k_0	3.18×10^9 s^{-1}	1.96×10^9
	Activation energy, E_A	1.17 eV/atom	0.10
Papazian II	Pre-exponential coefficient, k_0	1.05×10^9 s^{-1}	7.06×10^7
	Activation energy, E_A	1.26 eV/atom	0.15

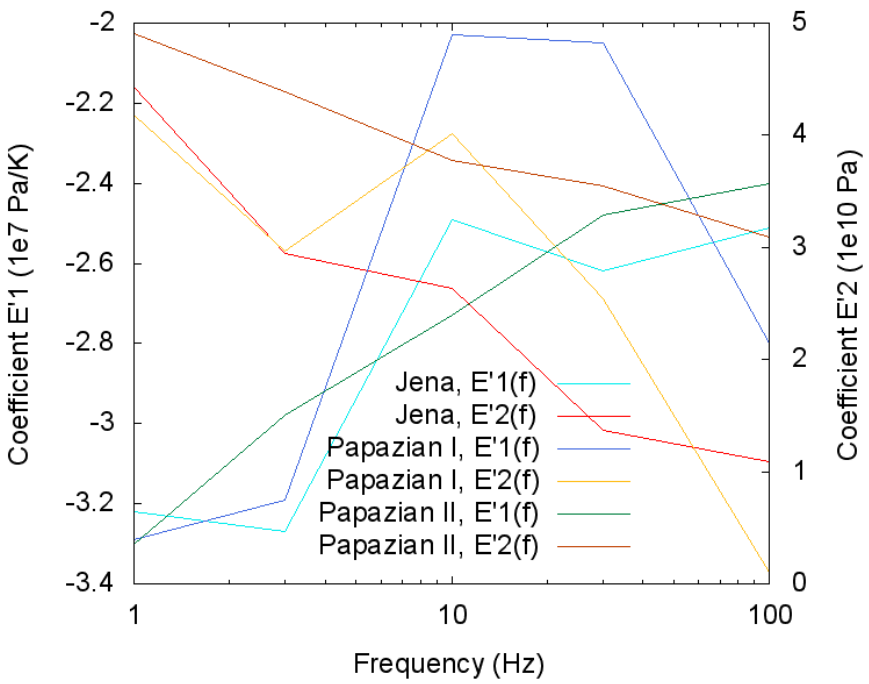

Fig. 8 Coefficients E'_1 and E'_2 of the proposed storage modulus model, computed through integration and fitting for three different types of transformation rate equations, for the case of AA 7075-T6.

4.1.4 Discussion of experimental and numerical results

The experimental results confirmed that the viscoelastic response depends on temperature and frequency of the mechanical excitation. The initial decrease in the storage modulus can be fairly explained by the dependence of the elastic moduli (elastic stiffness constants) on temperature, which is a well known phenomenon for metals, and particularly aluminium [42-45]. According to the results in the literature, it is reasonable to assume that the elastic modulus decreases linearly with temperature in the studied temperature range. We assumed that the storage modulus also decreases linearly with temperature, for modelization purposes, and the initial value used for E'_1 for the fitting procedures was very close to the slopes reported in the literature.

We ascribe the observed change in the storage modulus slope at 130-160 ºC to GPZ decomposition, given that GPZ dissolve around these temperatures [19, 22], and that the mechanical response of AlZnMg alloys below 220 ºC is controlled by the presence and decomposition of GPZ [13]. As temperature increases, the relaxation behaviour becomes more prominent, i.e. the storage and loss moduli vary more significantly with the frequency of the mechanical excitation at high temperatures. This phenomenon has also been observed in amorphous alloys [8]. Finally, the fact that the decrease in storage modulus at low frequencies is larger is typically explained by the reduction of the mechanical relaxation time as temperature increases [1, 8]. At low frequencies, the short relaxation time causes response with large phase lag, which results in a greater decrease of the storage modulus.

We proposed a model for the storage modulus as a function of temperature, frequency of the dynamic loading and GPZ concentration. We assumed that the driving mechanism of the GPZ dissolution was the same all along the transformation, and we used different models to express the GPZ dissolution rate. It can be concluded that the storage modulus model fits the experimental results reasonably well within the prescribed region of validity. In particular, the change in slope at

130-160 ºC is properly accounted for. This change and a rapid decrease in the computed GPZ concentration occur simultaneously and within a temperature interval in agreement with the reported window at which GPZ dissolution takes place [19, 22]. Hence, we consider that the numerical results support the hypothesis of the variation in the storage modulus slope at 130-160 ºC being caused by GPZ dissolution.

The values of the pre-exponential coefficient and the activation energy of the transformation rate equation for the GPZ dissolution are in good agreement with values reported in the literature by researchers using other techniques [15, 19, 22, 25, 28-30]. This fact confirms the validity of our numerical results for GPZ concentration with temperature, and indicates that the DMA and the proposed approach can be considered a good tool for studying the material microstructure and the kinetics of such phase transformations. Finally, it is noted that the pure Arrhenius dependence proposed by Jena and the 3D diffusion controlled rate expression proposed by Papazian describe similarly well the GPZ dissolution process, better than the first order diffusion expression also proposed by Papazian.

4.2 FUTURE WORK

In this section, a summary of the planned future work to achieve the thesis objectives is presented. Again, as much as it is possible, the tasks are presented in a hypothetical temporal order. Some of the tasks might be already in progress but at an early or middle stage and are not close yet close to completion.

1. An identical study is being conducted for AA 2024-T3 as the one reported for AA 7075-T6 through Sections 4.1.2 to 4.1.4.
2. We will consider whether it is interesting or not to cross-check more models for the GPZ dissolution rate equation, aside from Jena's and Papazian's.
3. We want to perform more dynamic-mechanical tests with the DMA and other equipments:
    a. We are currently performing new experiments with the DMA to determine the reversibility/elasticity or irreversibility/inelasticity of the processes taking place in our previous experiments for measuring the viscoelastic response (e.g. creation and motion of dislocations).
    b. We intend to perform other types of DMA tests as reported in papers [46], considering the TTS principle. That is, under isothermal conditions, we will measure the storage and loss moduli for AA 7075-T6 and AA 2024-T3 for frequencies ranging from 0.1 to 100 Hz, at temperatures ranging from 200 to 380 ºC in steps of 10 ºC.
    c. We have been trying to perform DMA tests at frequencies equal or slightly higher than the minimum nominal frequency of the DMA (0.01 Hz), and at frequencies equal or slightly smaller than the maximum nominal frequency of the DMA (200 Hz). The results of these tests do not seem very reliable to us, so we intend to obtain data for AA 7075-T6 and AA 2024-T3 at 0.01 Hz and lower frequencies using a Universal Testing Machine (UTM), if feasible, and data at frequencies higher than 200 Hz using ultrasound techniques.
    d. We intend to perform DMA tests on AA 7075 and AA 2024 samples with treatments different from the T6 and T3 tempers. The goal is to determine the differences in viscoelastic behaviour due to the temper or heat-treatment of the alloy.
    e. We will perform fatigue tests with the UTM that together with the DMA tests, will allow us to ascertain the influence of the frequency of dynamic loading on fatigue and its relationship with the viscoelastic behaviour.
4. We want to measure on our samples the values of GPZ concentration and the evolution of other microstructural features (e.g. the grain size and the content of other precipitates) with temperature in our samples. To achieve this:

   a. We have recently performed DSC scans on AA 7075-T6 samples previously heated at 1ºC/min from 35 to 100, 150, 200, 250, 300 and 400 ºC, respectively. These thermograms will be compared to data available in the literature, and will be correlated to DMA data. We intend to perform identical DSC scans on AA 2024-T3 samples.
   b. We intend to perform X-Ray Diffraction (XRD) tests on the as-received alloys, and in samples heated up to 100, 125, 150, 175, 200, 225, 250, 275, 300 and 400 ºC.
   c. We are currently performing optical microscopy observations of AA 7075-T6 samples heated from 35 to 50, 80, 100, 125, 150, 175, 200, 225, 250, 275, 300 and 400 ºC, respectively. We intend to perform identical tests on AA 2024-T3 samples.
   d. If necessary and possible, we will observe our samples, especially the GPZ, by Scanning Electron Microscope (SEM) or TEM
   e. If necessary and possible, we will observe our samples, especially the GPZ, by High Resolution TEM (HRTEM).
5. We will continue the study of the relations between the temperature, the frequency of the dynamic loading, the microstructure and the viscoelastic response and fatigue behaviour:
   a. We will run new simulations with the measured values of GPZ concentration.
   b. We will search for patterns in the behavior of E'_1 with frequency. As per now, our results partially agree with the theory and experimental results available in the literature, that state that E_1' should be less negative (i.e. should increase) with frequency. The differences might have arisen due to experimental errors.
   c. We will search for patterns in the behavior of E'_2 with frequency. As per now, E'_2 diminishes with increasing frequency. This suggests that at lower frequencies of excitation GPZ are stiffer than at higher frequencies, which might indicate that at lower frequencies the excited regions of the material are larger than the GPZ and at higher frequencies the excited regions are smaller than the GPZ.
   d. We will analyze why, for AA 7075-T6 and AA 2024-T3 at low temperatures, the loss modulus is lower for lower frequencies of mechanical excitation, while on the contrary at higher temperatures the plastic component of the viscoelastic response is lower for higher frequencies. To the author's knowledge, the latter behaviour is expected but the former is not. We will check whether this phenomenon is related to the grain size.
6. We will try to obtain the viscoelastic spectra from the experimental response functions. For instance, we already identified a peak in the plot of the loss modulus vs. frequency at 365ºC. The peak corresponds to a frequency and mechanical relaxation time of 2.51 Hz and 0.06 s, respectively.
7. We will try to find out whether the sizes of the excited regions in the material depend on the frequency of the mechanical excitations and how.
8. We will try to build a new model or refine the model previously presented, Eq. 6, such that it represents appropriately the viscoelastic behaviour over a wider range of temperatures, i.e. such that it includes the effects of phase transformations occurring at higher temperatures, like η' formation and dissolution, for example.
9. Ultimately, we might be able to develop an analytical model that relates the viscoelastic response of the alloys to their fatigue behaviour.

4.3 TENTATIVE CALENDAR

Finally, a Gantt diagram depicting the tentative calendar for the completion of the various tasks associated to the PhD thesis is shown (see Fig. 7). Major tasks are listed there as well as the expected time for the beginning and the end of the corresponding task.

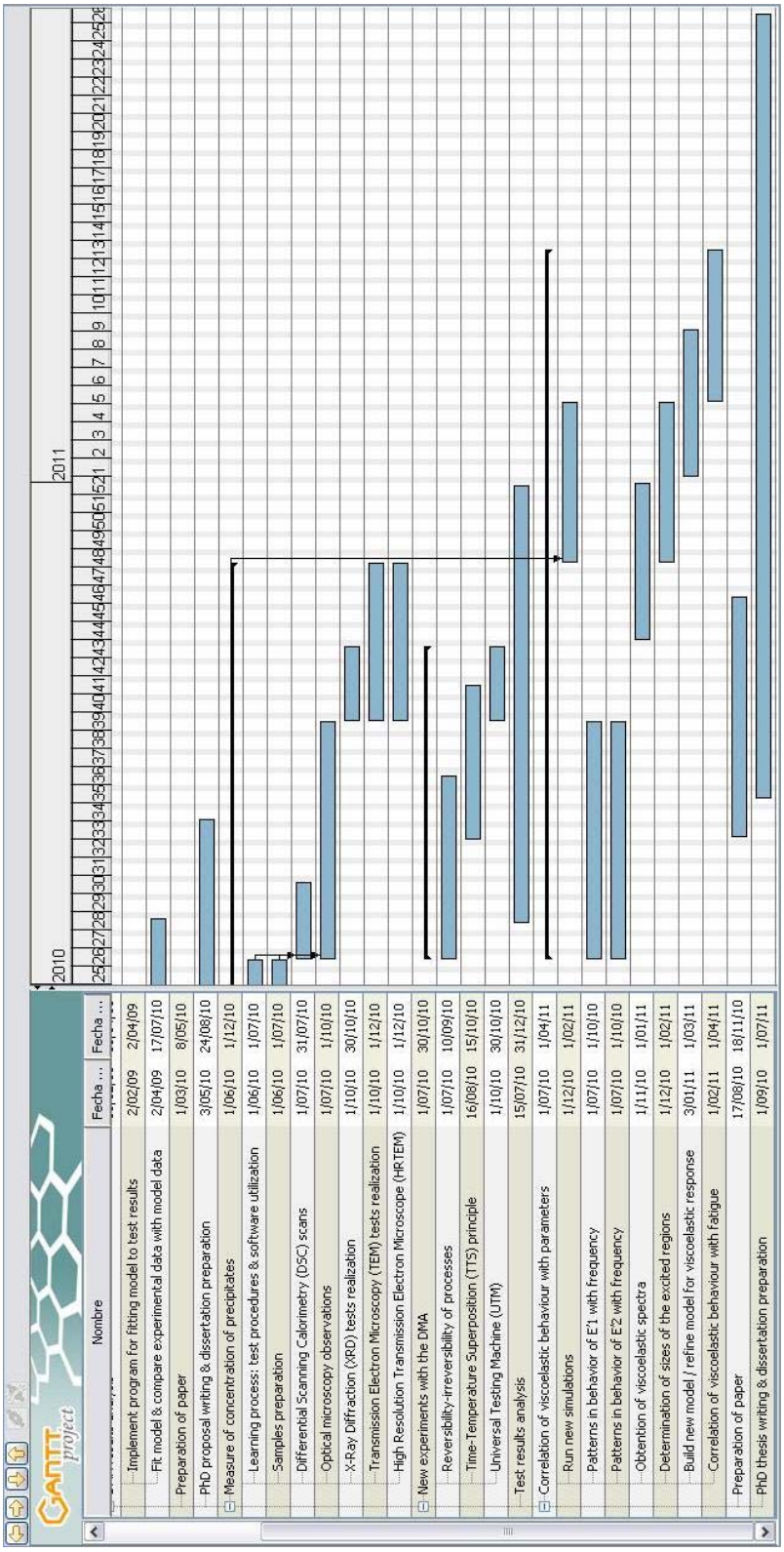

Fig. 9 Gantt diagram depicting the tentative calendar for the completion of the various tasks associated to the PhD thesis.

4.4 FUNDING

The proposed thesis is funded by the MINCIN grant MAT2010-14907 and the Generalitat de Catalunya grant 2009SGR01251.

4.5 PUBLICATIONS

The following publications resulted already from this research work:

- Rojas, J.I., Aguiar, A. and Crespo, D. *Effect of temperature and frequency of dynamic loading in viscoelastic properties of aluminium alloys AA 2024-T3 and 7075-T6*. Poster presented at IWNCS 2010, Barcelona (Spain), April 2010.
- Rojas, J.I., Aguiar, A. and Crespo, D. *Effect of temperature and frequency of dynamic loading in the viscoelastic properties of aluminium alloy 7075-T6*. This paper was submitted to *Physica Status Solidi* on July 22, 2010, and is currently under review. Publication is expected in early 2011.

5 EXECUTIVE SUMMARY

The mechanical properties of materials (and particularly the viscoelastic properties) are intimately linked to their microstructure [9, 10]. Thereby, microstructural transformations are reflected on the viscoelastic behaviour. Fatigue, for instance, is a consequence of microstructural changes induced by the viscoelastic response of a material under repeated loading. Accordingly, the characterization of the viscoelastic response of a material offers an alternative method for analyzing the microstructure, phase transformations (e.g. nucleation and growth, precipitate redissolution) and fatigue behaviour, aside from enabling a deeper understanding of other technologically essential properties, like damping, yielding, etc [1].

In the present work, the viscoelastic behaviour of commercial AlZnMgCu alloys is studied by means of dynamic-mechanical analysis, and the results are combined with calorimetric data and optical and electron microscopy data. These alloys are suitable to a number of industrial applications, and are of particular importance in the aerospace sector and transport industry.

This research is aimed at the identification and characterization of the effects of temperature, frequency of dynamic loading, microstructure and phase transformations on the viscoelastic behaviour of the mentioned alloys and the mechanical relaxation processes taking place. Ultimately, this research pursues to characterize the relation between the viscoelastic response of AlZnMgCu alloys under given operational conditions and their fatigue behaviour.

LIST OF ACRONYMS

AA	Aluminium Alloy
bcc	body-centered cubic
CCD	Charge-Coupled Device
CRAE	Centre de Recerca de l'Aeronàutica i de l'Espai
DEA	Advanced Studies Diploma
DIC	Differential Isothermal Calorimeter (or Calorimetry)
DMA	Dynamo-Mechanical Analyzer (or Analysis)
DoCTA	Doctorat en Ciència i Tecnologia Aeroespacial
DSC	Differential Scanning Calorimeter (or Calorimetry)
EPSC	Escola Politècnica Superior de Castelldefels
ETSIA	Escuela Técnica Superior de Ingenieros Aeronáuticos
fcc	face-centered cubic
GCM	Grup de Caracterització de Materials
GPBZ	Guinier-Preston-Bagariastkij Zones
GPZ	Guinier-Preston Zones
HB	Brinell hardness
HR	Rockwell hardness
HRTEM	High Resolution Transmission Electron Microscope (or Microscopy)
HV	Vickers hardness
RRA	Retrogression and Re-Ageing
RT	Room Temperature
SEM	Scanning Electron Microscope (or Microscopy)
SSS	(Super) Saturated Solid Solution
TEM	Transmission Electron Microscope (or Microscopy)
TTS	Time-Temperature Superposition
UPC	Universitat Politècnica de Catalunya
UTM	Universal Testing Machine
XRD	X-Ray Diffraction

REFERENCES

[1] Nowick, A.S., and Berry, B.S., "Anelastic relaxation in crystalline solids," Academic Press, New York; London, 1972, pp. 677.

[2] Abis, S., Massazza, M., Mengucci, P., *Scripta Materialia,* Vol. 45, No. 6, 2001, pp. 685-691.

[3] Bierwagen, G., "Next generation of aircraft coatings systems," *Journal of Coatings Technology,* Vol. 73, No. 915, 2001, pp. 45-52.

[4] Vreugdenhil, A.J., Balbyshev, V.N., and Donley, M.S., *Journal of Coatings Technology,* Vol. 73, No. 915, 2001, pp. 35-43.

[5] Starke, E.A., and Staley, J.T., *Progress in Aerospace Sciences,* Vol. 32, No. 2-3, 1996, pp. 131-172.

[6] Meyers, M.A., and Chawla, K.K., "Mechanical Behavior of Materials," Cambridge University Press, Cambridge, UK, 2009,

[7] Suh, D.W., and Dauskardt, R.H., *Journal of Materials Research,* Vol. 17, No. 6, 2002, pp. 1254-1257.

[8] Jeong, H.T., Fleury, E., Kim, W.T., *Journal of the Physical Society of Japan,* Vol. 73, No. 11, 2004, pp. 3192-3197.

[9] Karaaslan, A., Kaya, I., and Atapek, H., *Mp Materials Testing-Materials and Components Technology and Application,* Vol. 50, No. 5, 2008, pp. 256-258.

[10] Li, J.F., Peng, Z.W., Li, C.X., *Transactions of Nonferrous Metals Society of China,* Vol. 18, No. 4, 2008, pp. 755-762.

[11] Callister, W.D., "Materials science and engineering: an introduction," John Wiley, New York etc., 1985, pp. 602.

[12] Engdahl, T., Hansen, V., Warren, P.J., *Materials Science and Engineering A-Structural Materials Properties Microstructure and Processing,* Vol. 327, No. 1, 2002, pp. 59-64.

[13] Macchi, C.E., Somoza, A., Dupasquier, A., *Acta Materialia,* Vol. 51, No. 17, 2003, pp. 5151-5158.

[14] Viana, F., Pinto, A.M.P., Santos, H.M.C., *Journal of Materials Processing Technology,* Vol. 93, 1999, pp. 54-59.

[15] Ferragut, R., Somoza, A., and Dupasquier, A., *Journal of Physics-Condensed Matter,* Vol. 8, No. 45, 1996, pp. 8945-8952.

[16] Smith, G.W., *Thermochimica Acta,* Vol. 317, No. 1, 1998, pp. 7-23.

[17] Abis, S., Mengucci, P., and Riontino, G., *Materials Science and Engineering A-Structural Materials Properties Microstructure and Processing,* Vol. 214, No. 1-2, 1996, pp. 153-160.

[18] Badini, C., Marino, F., and Verne, E., *Materials Science and Engineering A-Structural Materials Properties Microstructure and Processing,* Vol. 191, No. 1-2, 1995, pp. 185-191.

[19] Jena, A.K., Gupta, A.K., and Chatuverdi, M.C., *Acta Metallurgica Et Materialia,* Vol. 37, No. 3, 1989, pp. 885-895.

[20] Gersten, J.I., and Smith, F.W., "The Physics and chemistry of materials," John Wiley & Sons, Inc., New York, NY, USA, 2001, pp. 826.

[21] Christian, J.W., "The Theory of transformations in metals and alloys," Pergamon, Oxford, etc., 2002, pp. 1113.

[22] Papazian, J.M., *Metallurgical Transactions A-Physical Metallurgy and Materials Science,* Vol. 13, No. 5, 1982, pp. 761-769.

[23] Kingery, W.D., Bowen, H.K., and Uhlmann, D.R., "Introduction to ceramics," John Wiley and Sons, New York, NY etc., 1976, pp. 1032.

[24] Hilliard, J.E., Averbach, B.L., and Cohen, M., *Acta Metallurgica,* Vol. 7, No. 2, 1959, pp. 86-92.

[25] Yannacopoulos, S., Kasap, S.O., Hedayat, A., *Canadian Metallurgical Quarterly,* Vol. 33, No. 1, 1994, pp. 51-60.

[26] Juhasz, A., Lendvai, J., and Kovacs, I., *Crystal Research and Technology,* Vol. 20, No. 3, 1985, pp. 401-405.

[27] Ceresara, S., and Fiorini, P., *Materials Science and Engineering,* Vol. 10, No. 4, 1972, pp. 205-&.
[28] Batra, U., and Prabhakar, S.R., *Transactions of the Indian Institute of Metals,* Vol. 48, No. 1, 1995, pp. 55-61.
[29] Dupasquier, A., Folegati, P., Rolando, A., *Materials Science Forum,* Vol. 175-178, 1995, pp. 351-354.
[30] Tankins, E.S., and Frazier, W.E., *Materials Performance,* Vol. 26, No. 6, 1987, pp. 37-44.
[31] Papazian, J.M., *Metallurgical Transactions A-Physical Metallurgy and Materials Science,* Vol. 12, No. 2, 1981, pp. 269-280.
[32] Starink, M.J., and Vanmourik, P., *Materials Science and Engineering A-Structural Materials Properties Microstructure and Processing,* Vol. 156, No. 2, 1992, pp. 183-194.
[33] Bhadeshia, H.K.D.H., "Differential Scanning Calorimetry,"
[34] Spence, J.C.H., "High-resolution electron microscopy," Oxford University Press, Oxford, UK, 2003, pp. 401.
[35] De Graef, M., "Introduction to conventional transmission electron microscopy," Cambridge University Press, Cambridge, UK, 2003, pp. 718.
[36] Hull, A.W., *Journal of the American Chemical Society,* Vol. 41, No. 8, 1919, pp. 1168-1175.
[37] Suryanarayana, C., and Grant Norton, M., "X-Ray Diffraction: a practical approach," Plenum Press, New York, NY, USA, 1998, pp. 273.
[38] Sharma, M.M., Amateaub, M.F., and Eden, T.J., *Journal of Alloys and Compounds,* Vol. 416, No. 1-2, 2006, pp. 135-142.
[39] Park, J.K., and Ardell, A.J., *Metallurgical Transactions A-Physical Metallurgy and Materials Science,* Vol. 14, No. 10, 1983, pp. 1957-1965.
[40] Graf, R., Polmear, I.J., Thomas, G., *Journal of the Institute of Metals,* Vol. 86, No. 13, 1958, pp. 535-538.
[41] Lyman, C.E., and Vandersande, J.B., *Metallurgical Transactions A-Physical Metallurgy and Materials Science,* Vol. 7, No. 8, 1976, pp. 1211-1216.
[42] Sutton, P.M., *Physical Review,* Vol. 91, No. 4, 1953, pp. 816-821.
[43] Kamm, G.N., and Alers, G.A., *Journal of Applied Physics,* Vol. 35, No. 2, 1964, pp. 327-330.
[44] Brammer, J.A., and Percival, C.M., *Experimental Mechanics,* Vol. 10, No. 6, 1970, pp. 245.
[45] Varshni, Y.P., *Physical Review B,* Vol. 2, No. 10, 1970, pp. 3952-3958.
[46] Jeong, H.T., Kim, J.H., Kim, W.T., *Materials Science and Engineering A-Structural Materials Properties Microstructure and Processing,* Vol. 385, No. 1-2, 2004, pp. 182-186.